energies

MDPI

Article

Development of a Hydrogen Fuel Cell Hybrid Urban Air Mobility System Model Using a Hydrogen Metal Hydride Tank

Sanghyun Yun [1], Seok Yeon Im [2,*] and Jaeyoung Han [1,3,4,*]

[1] Department of Mechanical Engineering, Kongju National University, 1223-24 Cheonan-daero, Cheonan-si 31080, Republic of Korea; m40984334@gmail.com
[2] Mechanical Engineering Education Department, Chungnam National University, Daejeon 34134, Republic of Korea
[3] Department of Future Automotive Engineering, Kongju National University, 1223-24 Cheonan-daero, Cheonan-si 31080, Republic of Korea
[4] Institute of Green Car Technology, Kongju National University, 1223-24 Cheonan-daero, Seobuk-gu, Cheonan-si 31080, Republic of Korea
* Correspondence: imsy@cnu.ac.kr (S.Y.I.); hjyt11@kongju.ac.kr (J.H.)

Abstract: Hydrogen fuel cell-based UAM (urban air mobility) systems are gaining significant attention due to their advantages of higher energy density and longer flight durations compared to conventional battery-based UAM systems. To further improve the flight times of current UAM systems, various hydrogen storage methods, such as liquid hydrogen and hydrogen metal hydrides, are being utilized. Among these, hydrogen metal hydrides offer the advantage of high safety, as they do not require the additional technologies needed for high-pressure gaseous hydrogen storage or the maintenance of cryogenic temperatures for liquid hydrogen. Furthermore, because of the relatively slower dynamic response of hydrogen fuel cell systems compared to batteries, they are often integrated into hybrid configurations with batteries, necessitating an efficient power management system. In this study, a UAM system was developed by integrating a hydrogen fuel cell system with hydrogen metal hydrides and batteries in a hybrid configuration. Additionally, a state machine control approach was applied to a distribution valve for the endothermic reaction required for hydrogen desorption from the hydrogen metal hydrides. This design utilized waste heat generated by the fuel cell stack to facilitate hydrogen release. Furthermore, a fuzzy logic control-based power management system was implemented to ensure efficient power distribution during flight. The results show that approximately 43% of the waste heat generated by the stack was recovered through the tank system.

Keywords: hybrid system; metal hydride tank; polymer electric membrane fuel cell; power management system; thermal management system; urban air mobility

Academic Editor: Zhenzhen Jin

Received: 24 November 2024
Revised: 17 December 2024
Accepted: 24 December 2024
Published: 26 December 2024

Citation: Yun, S.; Im, S.Y.; Han, J. Development of a Hydrogen Fuel Cell Hybrid Urban Air Mobility System Model Using a Hydrogen Metal Hydride Tank. *Energies* **2025**, *18*, 39. https://doi.org/10.3390/en18010039

1. Introduction

1.1. Research Background

Urban air mobility (UAM) is gaining significant attention as an innovative solution to environmental challenges arising from technological advancements and urban centralization, while also alleviating traffic congestion in cities. UAM has the potential to improve travel times, reduce road traffic accidents, and mitigate air pollution [1–3]. Currently, UAM systems primarily rely on lithium-ion batteries as power sources due to their technological maturity, safety, regulatory compliance, and suitability for short-term operations. However, lithium-ion batteries face limitations in meeting the increased power demands of manned

flights and enabling extended flight durations, primarily due to challenges such as state-of-charge (SOC) management and low energy density. To overcome these limitations, recent research has focused on UAM systems incorporating hydrogen fuel cell systems. Hydrogen fuel cells offer several advantages over batteries, including higher energy density, faster refueling times, and efficient long-range operation [4–6]. Among various types of fuel cells, such as polymer electrolyte fuel cells (PEFCs), phosphoric acid fuel cells (PAFCs), and solid oxide fuel cells (SOFCs), PEFCs are predominantly used in mobility applications because of their high power density, fast response, and low operating temperatures [7–10]. Fuel cells generate electricity through an electrochemical reaction between hydrogen and oxygen, making a consistent supply of these gases essential. In this process, the polymer electrolyte membrane, a key component of fuel cells, plays a central role in determining the system's performance and efficiency. The membrane selectively transports protons (hydrogen ions) generated from the dissociation of hydrogen molecules at the anode to the cathode while separating electrons to flow through an external circuit. This allows the protons to combine oxygen at the cathode to form water, completing the energy generation process. Such functionality of the membrane is crucial for ensuring the continuity and efficiency of the electrochemical reaction [11]. Currently, most hydrogen supply systems store hydrogen in the gaseous form at high pressure within tanks. However, alternative hydrogen storage and supply methods, including liquid hydrogen and metal hydride tanks, have been the subject of recent research [12–17]. Metal hydride tanks, in particular, offer advantages such as high safety, high-density hydrogen storage, and space-saving characteristics due to their solid-state storage without requiring high-pressure conditions. Despite these advantages, metal hydride technologies are still in the development stage. These tanks require external heat input to convert stored hydrogen from its solid form to a gaseous state, necessitating a thermal management system capable of meeting the hydrogen supply flow rate requirements. Furthermore, the performance, efficiency, and stability of fuel cell systems are significantly influenced by temperature, making an effective thermal management system essential. Hybrid configurations combining fuel cells and batteries are widely adopted to improve output stability, enhance energy recovery, and increase system responsiveness. Such systems require a robust power management system (PMS) to appropriately distribute power demands between the fuel cell and the battery.

1.2. Research Survey

Research on transitioning from battery-based UAM systems to hybrid UAM systems integrating hydrogen fuel cell systems and batteries has been actively conducted. Ahluwalia et al. conducted an economic evaluation of fuel cell systems for eVTOL air taxis, referencing fuel cell systems and batteries developed for medium-duty vehicles. They identified key factors for successfully applying fuel cell systems to air taxis, including durability, lightweight design, safety, and aviation compatibility [18]. Kim et al. performed power and weight analyses for the conceptual design of a tiltrotor battery–fuel-cell hybrid propulsion UAM system and proposed a thermodynamic and heat-transfer-based design methodology for hydrogen tank selection [19]. An et al. presented a sizing methodology for UAVs using hybrid fuel cell and battery systems, employing an advanced sizing methodology to determine energy requirements for flight, which resulted in improved energy efficiency and flight performance [20]. Santos et al. evaluated performance requirements for applying fuel cell systems to UAVs, focusing on efficiency, lightweight design, and durability, and confirmed that fuel cell systems offer longer flight times and higher efficiency compared to batteries [21]. Boukoberine et al. reviewed various strategies and future prospects for UAV power and energy management systems, analyzing power management strategies involving different power sources, such as batteries and fuel cells, and emphasizing their

importance [22]. Fakhreddine et al. analyzed the technical and economic challenges of hydrogen fuel cell systems in transportation, presenting future prospects to address these challenges and highlighting hydrogen fuel cell systems as key next-generation eco-friendly power sources [23]. Kim et al. assessed the efficiency of hybrid UAM systems with fuel cells compared to battery systems and proposed power management strategies to enhance performance and efficiency while improving cost-effectiveness [24]. Furthermore, Mazzeo et al. conducted theoretical analyses and simulations of a 70 kW fuel cell system applicable to lightweight helicopters, evaluating its potential as an eco-friendly urban transport solution [25].

The power management system for hydrogen-fuel-cell–battery hybrid systems significantly impacts the performance, efficiency, and lifespan of the system by optimizing energy efficiency, prolonging the lifespan of the fuel cell and its balance of plant (BoP) components, and ensuring a stable power supply. Consequently, extensive research has been conducted on this topic. Jia et al. proposed a novel energy management strategy for fuel-cell–battery hybrid electric buses. This strategy optimizes system efficiency and extends its lifespan by preventing excessive fuel cell degradation and ensuring battery thermal stability, considering the health state of the fuel cell and thermal and lifespan constraints of the battery [26]. Zheng et al. developed an energy management strategy based on Pontryagin's minimum principle (PMP) to extend the fuel cell stack's lifespan in hybrid vehicles. The proposed strategy optimizes energy allocation by incorporating the degradation mechanisms of the fuel cell stack and evaluates the extension of the fuel cell's lifespan and its economic benefits through simulations [27]. Pereira et al. introduced a real-time nonlinear model predictive control (NMPC)-based strategy for energy management in fuel cell hybrid electric vehicles. Their strategy optimizes energy distribution between the fuel cell and battery by considering the dynamic characteristics of the vehicle and energy system constraints, improving fuel efficiency and extending battery lifespan [28]. Zhou et al. proposed a real-time cost-minimizing power allocation strategy based on model predictive control for fuel cell hybrid electric vehicles. This strategy calculates the energy costs of the fuel cell and battery, performing real-time optimal power allocation to achieve high fuel efficiency, prolonged battery lifespan, and minimized operating costs [29]. He et al. developed a cost-minimizing power allocation strategy for fuel-cell–battery hybrid electric buses, considering the lifespans of the fuel cell and battery. By evaluating battery lifespan and fuel cell degradation, the strategy minimizes operational costs through optimized power distribution [30].

With the growing interest in hydrogen fuel cell-based UAM systems, research on thermal management has been actively conducted. Chang et al. simulated three cooling systems—air cooling, liquid cooling, and pulsating heat pipe cooling—for hydrogen fuel cell systems in UAVs and comparatively analyzed their thermal management performance. The study confirmed that the liquid cooling system was the most efficient for thermal management in high-power regions, while pulsating heat pipe cooling was identified as a useful alternative for lightweight UAV applications [31]. He et al. proposed an online energy management strategy that integrates the efficiency and thermal management of fuel cells. They addressed the issue of performance degradation caused by heat generated during fuel cell operation, suggesting methods to extend the lifespan and maximize performance through an efficient thermal management system. The proposed system employs a real-time, data-based control algorithm to regulate the flow of coolant, pump operation, and radiator heat dissipation, simultaneously optimizing fuel consumption and temperature variations [32]. Anselma et al. proposed a thermal management optimization method using Dynamic Programming for fuel cell systems. They developed an efficient cooling strategy to prevent fuel cell stack overheating under various thermal load conditions during

operation. Notably, the dynamic programming algorithm determined the operating points of the cooling system under diverse driving conditions, minimizing hydrogen consumption and ensuring system stability [33]. Li et al. comprehensively reviewed research trends and application cases related to key components of hydrogen fuel cell systems. Their review covered the latest studies on the design and optimization of fuel cell stacks, hydrogen storage systems, and thermal management systems. In particular, thermal management systems were emphasized as critical factors influencing fuel cell efficiency and lifespan. Additionally, strategies for balancing heat dissipation performance, cost, and weight in cooling system design were discussed [34].

Research on metal hydride tanks is also actively being conducted because of their advantages, such as high hydrogen storage density, safety, and flexibility in hydrogen storage and supply systems. Darkrim et al. investigated the effects of carbon nanotube properties on hydrogen adsorption and storage efficiency, analyzing the surface modifications and structures of carbon nanotubes to optimize storage and adsorption rates, as well as suggesting future research directions [35]. Sakintuna et al. outlined the advantages and limitations of metal hydride tanks, emphasizing their high energy density and stability. They compared the characteristics and reactivity of various metal hydrides and suggested directions for technological development and practical applications [36]. Satheesh et al. evaluated the thermal performance and efficiency of heat pumps using metal hydrides with different reaction temperatures, proposing design optimizations for heat pump systems based on metal hydride tanks [37]. Park et al. developed an integrated system combining metal hydride absorption/desorption reactions with compressors to enhance heat transfer efficiency and performance coefficients, proposing design conditions to improve system energy efficiency and stability [38]. Kim et al. analyzed absorption/desorption reactions in metal hydride tanks based on ultra-insulated thermal wave propagation, evaluating energy conversion efficiency and proposing design and operation conditions for system implementation [39]. Kikkinides et al. modeled and optimized the dynamic characteristics of metal hydride tanks, simulating hydrogen absorption/desorption reactions based on thermodynamic principles, and analyzed design variables to improve storage capacity, reaction rates, and thermal management efficiency [40].

In this study, the development of a hydrogen fuel cell hybrid UAM system model utilizing a metal hydride tank presents an innovative approach not addressed in previous research. While studies on hybrid UAM systems using batteries and hydrogen fuel cells have been actively conducted, the integration of fuel cell systems incorporating metal hydride tanks and system-level power management and analysis based on such configurations are scarcely found in the literature. Therefore, this study developed a hybrid UAM system model utilizing a metal hydride tank and designed a mechanism to enable the desorption of solid-state hydrogen from the tank by utilizing waste heat from the fuel cell stack. This approach maximized the efficiency of waste heat utilization while integrating auxiliary cooling loops and valve state control to ensure system stability. Additionally, a fuzzy logic control-based power management system was implemented, enabling efficient power distribution based on the state of charge (SOC) of the battery and load power.

2. System Configuration

The schematic diagram of the hydrogen–electric UAM system can be seen in Figure 1. The power sources consist of a 138 kW fuel cell system and a 60 kWh battery, while the power conversion devices include DC–DC converters, and the propulsion system comprises thrust motors and propellers. The power required by the fuel cell system and battery fluctuates based on the demands of the power distribution system, resulting in different voltage levels. To convert the voltage to the 400 V operating voltage of the thrust

motor, DC–DC converters were applied to each power source. A unidirectional converter was used for the fuel cell, as it only generates power using hydrogen, while a bidirectional converter was implemented for the battery to enable both charging and discharging. These components regulate the voltage to a unified bus voltage applied to the thrust motor. The thrust motor generates the thrust needed for the UAM to overcome its load and ascend to higher altitudes. The power required by the thrust motor is supplied by the fuel cell and battery, with the power management system distributing power based on the overall system's power requirements and the battery's state of charge (SOC).

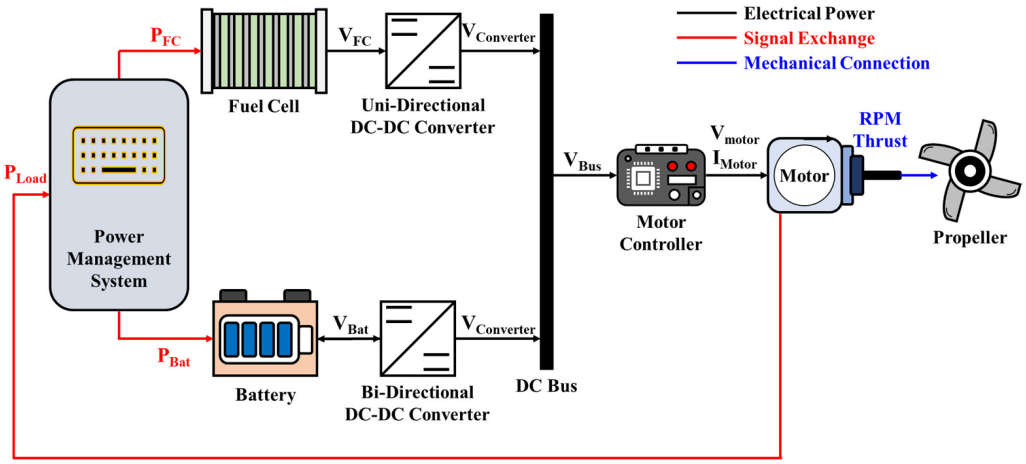

Figure 1. Schematic of the hydrogen fuel cell system–battery hybrid UAM system.

2.1. Fuel Cell System

The hydrogen fuel cell system comprises a stack that generates electricity through an electrochemical reaction between hydrogen and oxygen, along with a balance of plant (BOP) that ensures the stable operation of the stack. The BOP includes a hydrogen supply system and an air supply system to provide hydrogen and oxygen, respectively, as well as a thermal management system to dissipate the heat generated by the fuel cell stack, maintaining its optimal operating temperature.

2.1.1. Fuel Processing System

The hydrogen supply for stack operation is facilitated using a metal hydride tank, which, despite the drawback of requiring an external heat source, offers advantages such as a high hydrogen storage density per unit volume and enhanced safety. The heat transfer coefficient of the metal hydride tank was derived based on assumed heat transfer coefficients of metal hydrides and gaseous hydrogen, and it was modeled using thermodynamic and energy equations [41]. Figure 2 illustrates the schematic diagram of the metal hydride tank used in this study. The metal hydride tank consists of gaseous hydrogen and the metal hydride material $LaNi_5$, an alloy of lanthanum (La) and nickel (Ni) known for its high hydrogen affinity and ability to absorb and desorb hydrogen at low operating temperatures. These properties make $LaNi_5$ widely used in most metal hydride tanks. In this system, the metal hydride absorbs heat from an external heat source, enabling a desorption reaction that converts solid-state hydrogen into gaseous hydrogen, which is then supplied to the fuel cell stack.

The tank accounts for changes in the gaseous hydrogen density over time, hydrogen desorption from the metal hydride, and hydrogen release from the tank. The mass conservation equation for this system is expressed as follows:

$$\left(\frac{V_{tank}}{V_{MH}} - 1 + \varepsilon\right)\frac{\partial \rho^g}{\partial t} = \dot{m}'''_{MH} - \dot{m}'''_{out} \quad (1)$$

Here, $\frac{V_{tank}}{V_{MH}}$ represents the ratio of the tank volume to the metal hydride volume, and ε denotes the porosity; $\dot{m}'''_{MH}$ and $\dot{m}'''_{out}$ represent the mass flow rate per unit volume for the metal hydride and tank, respectively. The porosity accounts for the fact that metal hydride is not a completely solid material, allowing for a more precise calculation of the masses of the metal hydride and the gaseous hydrogen.

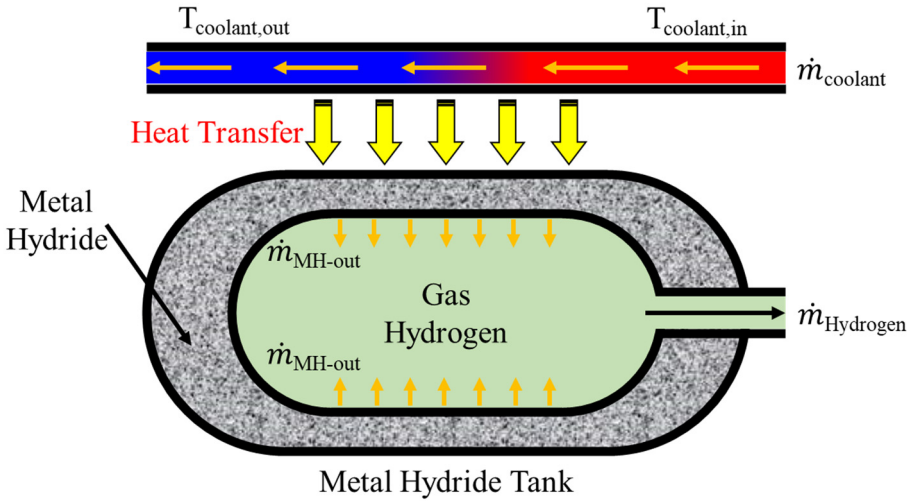

Figure 2. Schematic of a metal hydride tank.

Hydrogen desorption in the metal hydride can be expressed based on the heat transfer from an external heat source, heat transfer within the metal hydride tank, and a thermodynamics-based energy conservation equation, as shown below:

$$\left(\frac{V_{tank}}{V_{MH}} - 1 + \varepsilon\right) C_{pg} \frac{\partial(\rho^g T)}{\partial t} + (1-\varepsilon) C_{ps} \frac{\partial(\rho^s T)}{\partial t} = k_e \nabla^2 T - \dot{m}'''_{MH} \Delta H + \dot{Q}''' \quad (2)$$

Here, C_{pg} and C_{ps} represent the specific heat capacities of the gas and metal hydride, respectively, while ρ^g and ρ^s denote the densities of the gas and metal hydride. Additionally, k_e is the thermal conductivity of the metal hydride, ΔH represents the enthalpy change during the desorption process in the metal hydride, and $\dot{Q}'''$ indicates the heat input from an external source.

The mass flow rate of hydrogen generated during desorption in the metal hydride can be calculated using the Arrhenius equation, which is based on collision theory and the molecular kinetic energy required for the chemical reaction to occur.

$$\dot{m}'''_{MH} = -C_a exp\left(\frac{-E_A}{RT}\right) ln\left(\frac{P}{P_{eq}}\right)(\rho_s^s - \rho^s) \quad (3)$$

Here, $\dot{m}'''_{MH}$ represents the mass flow rate per unit volume from the metal hydride, C_a is the reaction coefficient determined by the physical and chemical properties of the metal hydride, and $-E_A$ denotes the activation energy required for hydrogen desorption from the metal hydride.

The pressure changes in the metal hydride tank can be expressed as follows, based on the thermodynamic relationship between hydrogen storage capacity and temperature, illustrating how hydrogen desorption occurs with temperature variations.

$$ln\frac{P_{eq}}{P_0} = a + \frac{b}{T} + (\phi \pm \phi_0) tan\left[\alpha_1 \pi \left\{\left(\frac{H}{H_{max}}\right) - \alpha_2\right\}\right] \pm \frac{\beta}{2} \quad (4)$$

Here, $ln\frac{P_{eq}}{P_0}$ represents the pressure ratio change during the hydrogen desorption process, a and b are coefficients that define how the equilibrium pressure in the metal hydride tank changes with the temperature, H is the current hydrogen storage level, and H_{max} is the maximum hydrogen storage capacity. Additionally, ϕ and ϕ_0 and α_1 and α_2 are physical property constants related to the adsorption mechanism of the metal hydride tank.

The flow rate of the gaseous hydrogen generated from the desorption in the metal hydride tank is determined by the tank's internal pressure, temperature, and flow characteristics (Mach number and specific heat ratio) and can be calculated as follows:

$$\dot{m}'''_{out} = \frac{P_{tank}}{V_{tank}\sqrt{RT_{tank}}} A_{th}\sqrt{r}Me\left(1+\frac{(r-1)Me^2}{2}\right)^{\frac{(r+1)}{(2-2r)}} \quad (5)$$

Here, P_{tank} represents the internal pressure of the tank, V_{tank} is the tank volume, A_{th} denotes the heat transfer area due to the external heat source, and Me represents the Mach number for hydrogen outflow.

The heat supplied by the external heat source is entirely transferred to the metal hydride tank, and the process is assumed to be adiabatic, with no natural convection occurring with the external environment.

$$dQ_{coolant} = UdA(T - T_{MH}) = -\dot{m}_{coolant}C_{p,coolant}dT \quad (6)$$

Here, $dQ_{coolant}$ represents the amount of heat transferred to the metal hydride tank, U is the heat transfer coefficient, and dA denotes the area through which the heat transfer occurs. Table 1 presents the list of parameters and data for the metal hydride tank developed in this study.

Table 1. Parameters for the metal hydride tank model [42].

System	Components	Parameters	Unit
Metal Hydride Tank	a	13.44	-
	b	3780	K
	α_1	1	-
	α_2	0.5	-
	β	0.137	-
	d_e	0.005	m
	D_{tank}	0.6	m
	L_{tank}	1	m
	C_a	59.187	1/s
	C_{pg}	14,890	J/kg·K
	C_{ps}	419	J/kg·K
	C_{pw}	1860	J/kg·K
	E_a	21,179.6	J/mol
	ΔH	1.54×10^7	J/kg
	ε	0.5	-
	γ	1.409	-
	ϕ	0.038	-
	ϕ_0	0	-
	ρ_{s0}	8400	kg/m^3
	ρ_{ss}	8517	kg/m^3
	R_u	8.314	J/mol·K
	U	300	$W/m^2 \cdot K$

2.1.2. Air Processing System

In this study, a pressurized compressor capable of maintaining a high supply pressure was applied to the high-capacity fuel cell system, which requires high power output. The

required supply pressure and flow rate for the stack are calculated as follows, and the developed compressor is controlled using a PI controller.

$$\dot{m}_{O_2} = \frac{i}{nF} \times n_{cell} \times stoi \tag{7}$$

$$P = \left(1 + \frac{\eta(\dot{m}, U)}{T_{atm} C_P}\right)^{\gamma/(\gamma-1)} \times P_{atm} \tag{8}$$

Here, $\dot{m}_{O_2}$ represents the required oxygen flow rate, F is the Faraday constant, i is the load current, and $stoi$ denotes the oxygen stoichiometric ratio.

2.1.3. Stack

The hydrogen fuel cell stack was developed based on Ballard's FCgen-HPS fuel cell stack, designed for low mass to meet the requirements of aerial mobility. The stack was validated through experimental studies, as shown in Figure 3 [43]. Detailed information about the stack can be found in Table 2. The voltage of the fuel cell stack is calculated by considering the theoretical maximum voltage determined by the temperature and fuel concentration, known as the Nernst voltage. This is adjusted by accounting for the activation losses caused by the energy required to initiate the electrochemical reaction, concentration losses due to fuel depletion at high current densities, and ohmic losses resulting from the system's electrical resistance and ionic conductivity, as expressed below:

$$V_{cell} = E - V_{act} - V_{con} - V_{ohm} \tag{9}$$

$$E = -\frac{\Delta g_f}{nF} = -\frac{\Delta g_f^0}{nF} + \frac{RT}{nF} ln\left(\frac{p_{H_2} p_{O_2}^{0.5}}{p_{H_2O}}\right) \tag{10}$$

$$V_{act} = \frac{RT}{n\alpha F} ln\left(\frac{j}{j_0}\right) \tag{11}$$

$$V_{conc} = \frac{RT}{nF} ln\left(1 - \frac{j}{j_L}\right) \tag{12}$$

$$V_{ohm} = i \times R_{ohm} \tag{13}$$

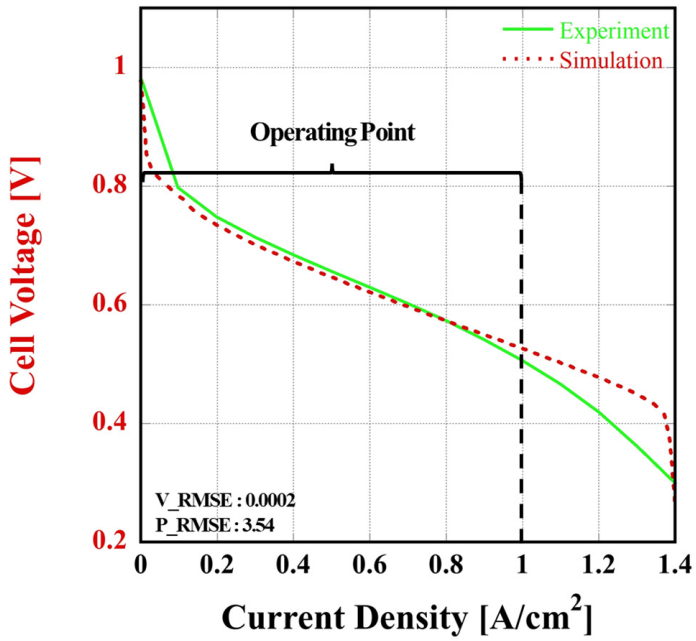

Figure 3. Polarization curve characteristic of a single fuel cell.

Table 2. FCgen-HPS fuel cell stack specifications [43].

System	Component	Parameter	Unit
Fuel Cell Stack	Rated power	138	kW
	Number of cells	309	ea
	Rated current	645	A
	Rated voltage	202	V
	Mass	55	kg
	Active area	480	cm^2

Here, Δg_f represents the change in Gibbs free energy, j is the current density, j_0 is the exchange current density, j_L is the limiting current density, and R_{ohm} denotes the internal resistance.

2.1.4. Thermal Management System

The fuel cell stack must maintain a stable operating temperature range to achieve an efficient performance, making the thermal management system essential. Additionally, this study proposes a mechanism to utilize the waste heat from the fuel cell to enable hydrogen desorption from the metal hydride tank. To effectively implement this mechanism, the flow and temperature of the coolant must be controlled through the thermal management system. Lastly, this study aims to develop an integrated model of a hydrogen fuel cell-based hybrid UAM system, and the thermal management system model is a critical component for simulating and optimizing the interactions between the fuel cell stack, metal hydride tank, coolant pump, and radiator.

Accordingly, in this study, the thermal management system removes the heat generated during the operation of the fuel cell stack to maintain the stack within its operating temperature range. It consists of a three-way valve, coolant pump, radiator, and cooling fan. Because of time and economic constraints, the development of each thermal management component was based on the experimental testing literature. Additionally, the heat required for the metal hydride tank is supplied via heat exchange using coolant heated by the fuel cell's operation. This is achieved through a separate distribution valve, as shown in Figure 4.

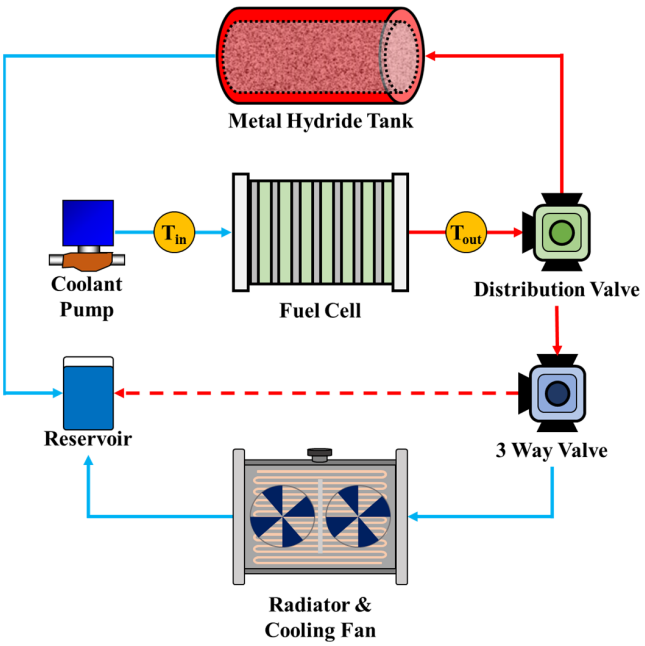

Figure 4. Thermal management system of the fuel cell stack and metal hydride tank.

The inlet and outlet temperatures of the stack are maintained at 333.15 K and 343.15 K, respectively, by controlling the inlet and outlet coolant temperatures using a PI controller for the cooling fan and coolant pump. Additionally, the distribution valve for the flow to the metal hydride tank ensures efficient heat transfer to the tank when the high-temperature coolant, which is sufficiently heated by the stack, enters. However, when the hydrogen flow rate required by the stack is low, the continuous desorption of the hydrogen from the metal hydride due to the high-temperature coolant can lead to instability in the tank. To address this, state machine control was applied to manage the distribution valve based on the stack's outlet coolant temperature and the hydrogen flow rate requirements. The state machine control operates by systematically and clearly defining actions based on input data, criteria, and rules. Accordingly, 12 states were defined based on the hydrogen flow rates and the stack's outlet coolant temperature, and the control was implemented as described in Table 3.

Table 3. State machine control of the distribution valve.

State	Stack Outlet Temperature [K]	Mole Flow Rate [mol/s]	Distribution Valve [-]
1	Low	$\dot{m} > \dot{m}_1$	Opening Ratio = 1
2	Low	$\dot{m} > \dot{m}_2$	Opening Ratio = 0.9
3	Low	$\dot{m} > \dot{m}_3$	Opening Ratio = 0.8
4	Low	$\dot{m} > \dot{m}_4$	Opening Ratio = 0.7
5	Medium	$\dot{m} > \dot{m}_1$	Opening Ratio = 0.8
6	Medium	$\dot{m} > \dot{m}_2$	Opening Ratio = 0.7
7	Medium	$\dot{m} > \dot{m}_3$	Opening Ratio = 0.6
8	Medium	$\dot{m} > \dot{m}_4$	Opening Ratio = 0.5
9	High	$\dot{m} > \dot{m}_1$	Opening Ratio = 0.6
10	High	$\dot{m} > \dot{m}_2$	Opening Ratio = 0.5
11	High	$\dot{m} > \dot{m}_3$	Opening Ratio = 0.4
12	High	$\dot{m} > \dot{m}_4$	Opening Ratio = 0.3

2.2. Battery

The battery serves as an auxiliary power source to complement the slow response speed of the hydrogen fuel cell system and meet the required power output. Additionally, it facilitates the load distribution, efficiency optimization, system stability, and operational flexibility, thereby improving the overall system's efficiency through organic power distribution during the system's operation [44–46]. Lithium-ion batteries are well-suited to hybrid UAM applications because of their unique charging and discharging characteristics, including high energy density, efficiency, and long cycle life. During the charging process, lithium ions move to the anode through the electrolyte, while during discharge, the ions move back to the cathode, releasing stored energy. Key factors influencing these processes include the battery's state of charge (SOC), temperature, and applied current, all of which significantly impact performance and lifespan. In this study, lithium-ion batteries, commonly used in electric vehicles, were scaled down based on experimental data for application in multicopter systems [47]. Furthermore, to accurately model the battery's characteristics, a 2-RC equivalent circuit model was developed to reflect its electrical and dynamic properties, as expressed below:

$$V_{BT} = V_{OC} - i \times \left\{ R_0 + R_1 \left(1 - e^{(-t/\tau_1)} \right) + R_2 \left(1 - e^{(-t/\tau_1)} \right) \right\} \quad (14)$$

Here, V_{OC} represents the open-circuit voltage of the battery, R_0 denotes the internal resistance of the battery, R_1 and R_2 represent the dynamic resistances within the battery, and τ_1 and τ_2 indicate the time constants.

2.3. DC–DC Converter

The DC–DC converter serves to convert the voltage generated by the hydrogen fuel cell system and battery into the operating voltage required by the motor. Through this process, the output voltage of the converter is supplied to the motor at a consistent voltage level. However, since the battery undergoes both discharging to power the motor and charging using the power generated by the fuel cell, a bidirectional DC–DC converter was applied. In this study, the converter was developed based on a duty ratio control method.

$$V_{Conv,out} = \frac{V_{Conv,in}}{1 - Duty\ ratio} \tag{15}$$

$$i_{Conv,out} = (1 - Duty\ ratio) \times i_{Conv,in} \tag{16}$$

Here, $V_{Conv,in}$ represents the input voltage to the converter, $V_{Conv,out}$ denotes the output voltage of the converter, and the $Duty\ ratio$ refers to the duty ratio.

2.4. Thrust Motor

The UAM system developed in this study was designed with a quadcopter structure, consisting of four propulsion motors, because of its simplicity, streamlined control system, and efficient power consumption. The propulsion motors were modeled using a first-order differential equation to describe the rotational speed as a function of the input current. The thrust was calculated based on the thrust coefficient of the propulsion motors, as formulated below.

$$\frac{d\omega}{dt} = \frac{K_t}{J} i - \frac{B}{J} \omega \tag{17}$$

$$F_{Thrust} = k_f \times \omega^2 \tag{18}$$

Here, ω represents the angular velocity of the motor, K_t denotes the motor torque constant, J is the moment of inertia, i is the input current, B represents the viscous friction coefficient, and k_f is the thrust coefficient. Detailed specifications of the propulsion motors can be found in Table 4.

Table 4. Specifications of the thrust motor with the blade.

Current [A]	Speed [RPM]	Thrust Force [N]	Power [kW]	Efficiency [%]
6.94	1166	250.84	2.33	83.57
12.46	1424	381.61	4.37	87.58
20.49	1684	538.67	7.38	89.94
33.39	1936	762.92	12.25	91.72
50.47	2197	1008.57	18.56	91.98
74.87	2449	1299.34	27.27	91.22
108.3	2703	1632.48	38.64	89.42

3. Results and Discussion

A power management system was implemented to evaluate the hybrid UAM system based on a hydrogen fuel cell system with an integrated metal hydride tank. Additionally, the flight simulation scenarios were designed based on the standards of South Korean aviation law to analyze the system's response and thermal management performance.

3.1. Power Management System

The power management system must ensure an efficient load distribution among power sources to maintain the system's stability and efficiency [48,49]. Additionally, the battery, which operates as an auxiliary power source, must maintain an optimal SOC while

meeting the required power demand. In this study, a fuzzy logic control-based power management system was developed to enable organic control across various system states. Fuzzy logic control defines each state for the input data and determines the degree of membership based on the membership functions. Subsequently, the inference result is calculated using fuzzy rules, and the result is transformed into system input data for control purposes, as defined below.

1. Fuzzification: the process of defining the proportions of the membership function to convert continuous and precise values into a fuzzy set that can be processed by fuzzy logic.
2. Fuzzy Inference: the process of applying predefined fuzzy rules to the fuzzified inputs to determine the degree of membership of their output values and calculate the final output.
3. Defuzzification: the process of converting the fuzzified output values into actual output values for the physical system.

Based on this approach, the power management system was designed to appropriately follow the load power while maintaining the battery's SOC within an optimal range. The load power for the fuel cell was determined using two input parameters, and the battery power was subsequently calculated based on the determined fuel cell power. The SOC of the battery was defined using the following states: Very Low, Low, Medium, High, and Very High. The membership functions were also defined accordingly. For the load power, the states were defined as follows: Off, Very Small, Small, Little Small, Medium, Little Large, Large, Very Large, and Max. Fuzzy Rules were then defined as shown in Table 5 and Figure 5. In this configuration, when the SOC is high, the power demand on the fuel cell decreases, while when the SOC is low, the load power handled by the fuel cell increases. Additionally, the power distribution ratio between the fuel cell and the battery was designed to vary depending on the total system load.

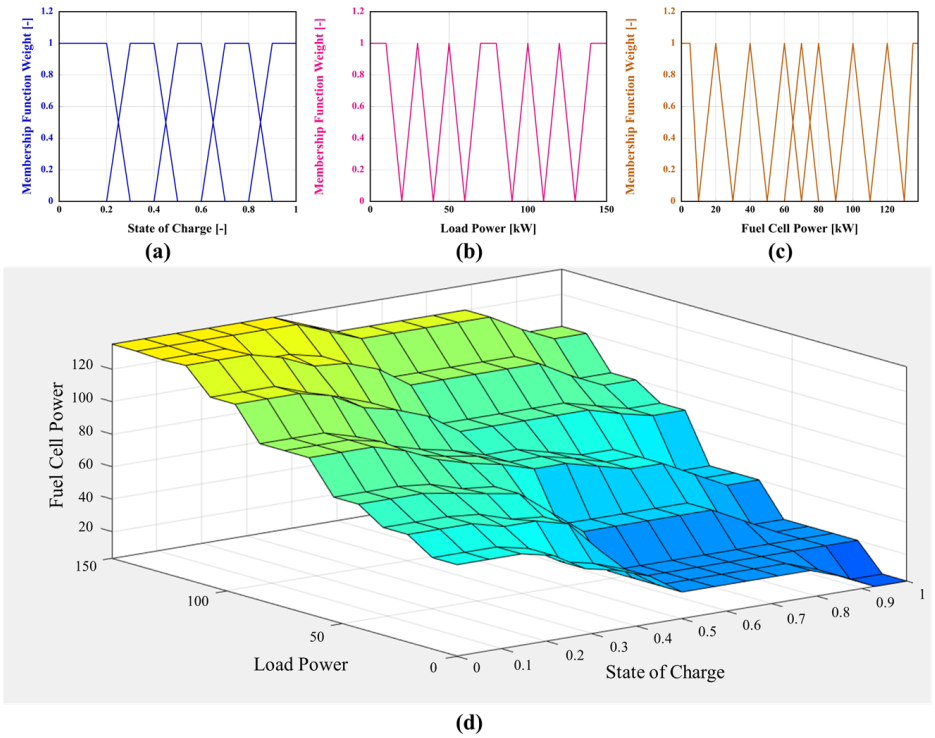

Figure 5. Fuzzy logic control: (**a**) membership function of the SOC; (**b**) membership function of the load power; (**c**) membership function of the fuel cell power; (**d**) 3D graph of the fuzzy logic control.

Table 5. Fuzzy rules of the power management system.

Fuzzy Rules of the PMS		Load Power [kW]						
		Off (0~20)	**Very Small (20~40)**	**Small (40~60)**	**Medium (60~90)**	**Large (90~110)**	**Very Large (110~130)**	**Max (130~150)**
State Of Charge [-]	**Very Low (~0.3)**	Little small	Medium	Little large	Large	Very large	Max	Max
	Low (0.3~0.5)	small	Little small	Medium	Little large	Large	Very large	Max
	Medium (0.4~0.7)	Very small	Very small	Small	Medium	Little large	Large	Very large
	High (0.6~0.9)	Very small	Very small	Small	Little small	Little large	Large	Very large
	Very High (0.8~)	Off	Very small	Very small	Small	Medium	Little large	Large

3.2. Flight Profile

Based on the fuzzy logic control power management system, the power of the fuel cell system with a metal hydride tank and the battery is distributed accordingly, and a flight simulation scenario was developed to analyze the system's behavior. The scenario was designed based on the operational concept document for Korean Urban Air Mobility (K-UAM) provided by the Ministry of Land, Infrastructure, and Transport of South Korea, with the altitude constraints set between 300 and 600 m. As shown in Figure 6, the simulation was developed to include the stages of takeoff, ascent, cruising, descent, and landing, reflecting the flight characteristics of UAM [50]. The simulation results confirm that the altitude of the hydrogen fuel cell hybrid UAM appropriately follows the changes in altitude during flight.

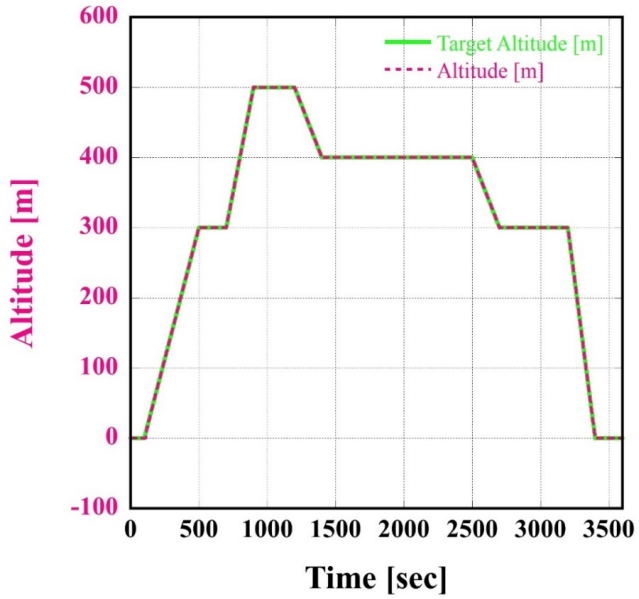

Figure 6. Hydrogen fuel cell hybrid UMA system in an altitude flight scenario.

3.3. Urban Air Mobility Performance

For flights at the target altitude, the UAM system ascends when the thrust generated by the propulsion motors exceeds the weight of the UAM system and descends when the thrust decreases. The mass of each component of the UAM system developed in this study

was assumed based on the reference literature, as shown in Table 6, and the altitude was calculated using the following equation [51]:

$$Altitude = \int \int (F_{Thrust} - F_{Gravity})dt \quad (19)$$

Table 6. Mass specifications of the hydrogen fuel cell hybrid UMA system.

Component	Mass [kg]
Fuel cell stack	55
DC–DC converter	15 × 2 ea
Hydrogen tank	72
Structure	120
Passenger	80
Thrust motor	9.1 × 4 ea
Battery	63
Total	462.4

Here, $Altitude$ represents the altitude, F_{Thrust} denotes the thrust generated by the propulsion motors, and $F_{Gravity}$ represents the gravitational force based on the mass of the UAM system. The thrust and gravity are illustrated in Figure 7. It was observed that the thrust generated by the propulsion motors varies and is controlled to achieve altitude control as the target altitude changes. In a hovering state, where there is no change in altitude, the thrust matches the gravitational force, maintaining a steady altitude.

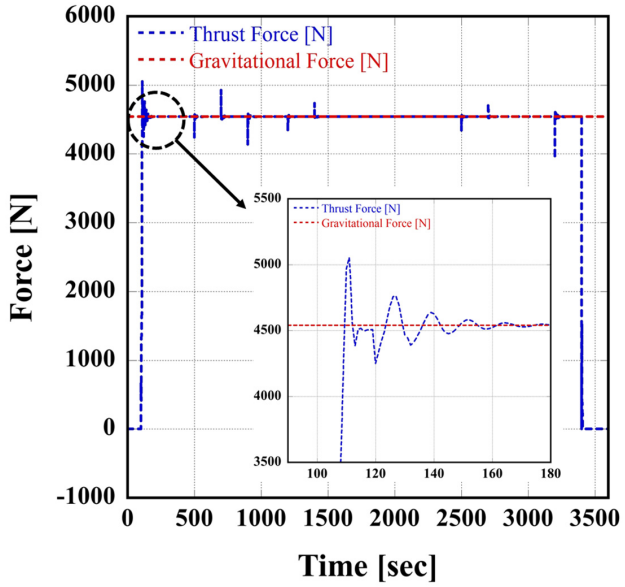

Figure 7. Thrust and gravitational force results of the hydrogen fuel cell hybrid UAM system.

3.4. Discussion

The required power for flight to the target altitude is distributed between the hydrogen fuel cell and the battery by the fuzzy logic control-based power management system, as shown in Figure 8. At the beginning of the flight, the increasing power demand is met by distributing the load between the fuel cell and the battery. As the battery's SOC decreases, the battery's load power organically adjusts according to the fuzzy rules. When the battery's SOC reaches 0.4, most of the load power is handled by the fuel cell, reducing the reliance on the battery. From the 3400 s mark, when the load power decreases, the power generated

by the fuel cell is directed to the battery for charging. According to the power management system, the load power from the hydrogen fuel cell system fluctuates, leading to variations in the required hydrogen flow rate. Consequently, the heat demand from the metal hydride tank varies, and the opening rate of the distribution valve is controlled by the state machine control, as shown in Figure 9. During the initial stage of the flight, because of the low operating temperature and hydrogen flow rate of the fuel cell system, the distribution valve operates in State 4 of the state machine control (Table 3). At the 100 s mark, with the start of flight and increased load power from the fuel cell, the temperature and hydrogen flow rate rise, transitioning to States 5 to 7. Furthermore, because of the high operating temperature of the fuel cell stack, the state transitions to State 10 and, subsequently, to State 9 as the hydrogen flow rate increases. Finally, at the end of the flight, as the fuel cell operates at low power to charge the battery, the hydrogen flow rate decreases, transitioning to State 12.

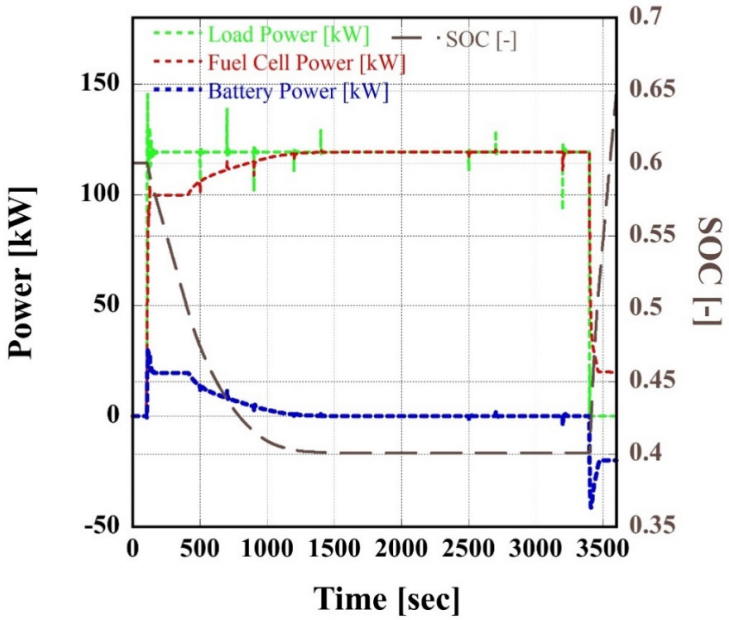

Figure 8. Power distribution and SOC with fuzzy logic control-based power management system.

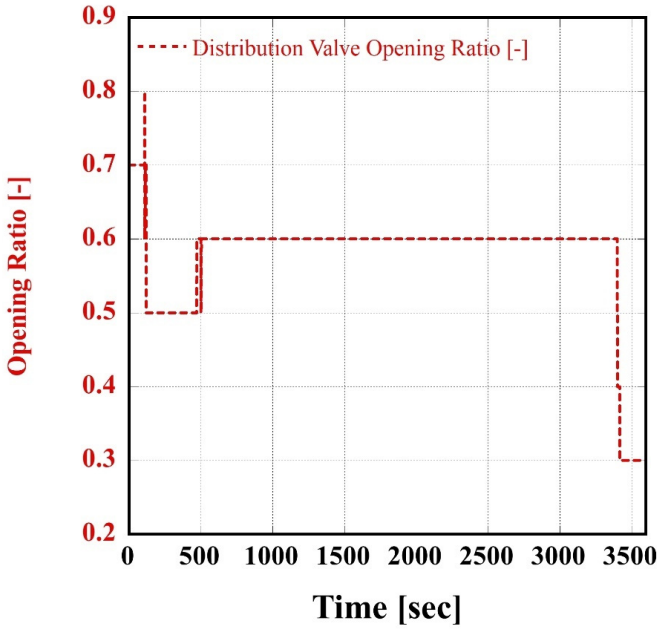

Figure 9. Results of the distribution valve with state machine control.

Through the distribution valve, the coolant flows into the metal hydride tank, causing the metal hydride to desorb hydrogen, converting it into gaseous hydrogen, which is then supplied to the fuel cell stack. To meet the required hydrogen flow rate, the outlet valve of the tank is controlled, as shown in Figure 10. During the flight, the hydrogen flow rate required for the operation of the hydrogen fuel cell system is controlled across all intervals by adjusting the valve opening rate. It can be observed that the required flow rate changes proportionally to the fuel cell's load power and is effectively tracked by the valve control system.

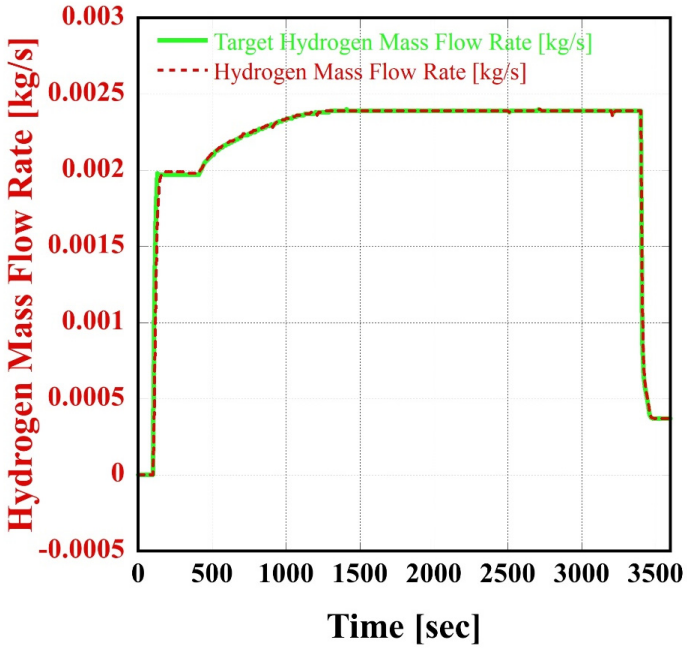

Figure 10. Hydrogen mass flow rate results with the mass flow rate control valve.

The high-temperature coolant heated by the stack is cooled by the distribution valve through the metal hydride tank and the radiator and cooling fan, and all of the coolant is mixed in the reservoir, reducing the temperature. However, the inlet and outlet temperatures of the stack are controlled to 333.15 and 343.15 K by the coolant pump and the cooling fan, which is confirmed in Figure 11. Figure 11a shows the inlet coolant temperature of the fuel cell stack. The high-temperature coolant heated by the stack is cooled by the distribution valve through the metal hydride tank and the radiator and cooling fan, and all of the coolant is mixed in the reservoir and the temperature is reduced. However, the inlet and outlet temperatures of the stack are controlled to 333.15 and 343.15 K by the coolant pump and the cooling fan, which can be confirmed through Figure 11. Figure 11a shows the inlet coolant temperature of the fuel cell stack, confirming that the temperature fluctuated according to the load change but was controlled to the target temperature of 333.15 K. In the first 500 s of the simulation, a section appeared where the temperature decreased rapidly. This was the result of the change in the opening rate of the distribution valve to the metal hydride tank. Before 500 s of the simulation elapses, the required flow rate of the hydrogen is low, so the opening rate of the distribution valve operates at 0.5. However, after 500 s, the required flow rate of the hydrogen increases, and the opening rate of the distribution valve operates at 0.6. Accordingly, the flow rate of the coolant flowing to the radiator decreases, but since the inlet temperature is still lower than the target temperature, the cooling fan operates at the same minimum flow rate, which is considered to be the temperature change. In addition, after 3400 s, as the load power of the fuel cell decreases, the required flow rate of the hydrogen decreases, and, accordingly, the opening rate decreases to 0.3 by

operating the state machine control of the distribution valve. Therefore, it is confirmed that the heat dissipation to the metal hydride tank decreases and the temperature increases accordingly, but it converges to the target temperature by controlling the cooling fan. In the case of Figure 11b, the temperature increases as the UAM flies in the 100 s section, but it is controlled to the target temperature by the coolant pump, and the temperature decreases as the load power of the fuel cell decreases after 3400 s.

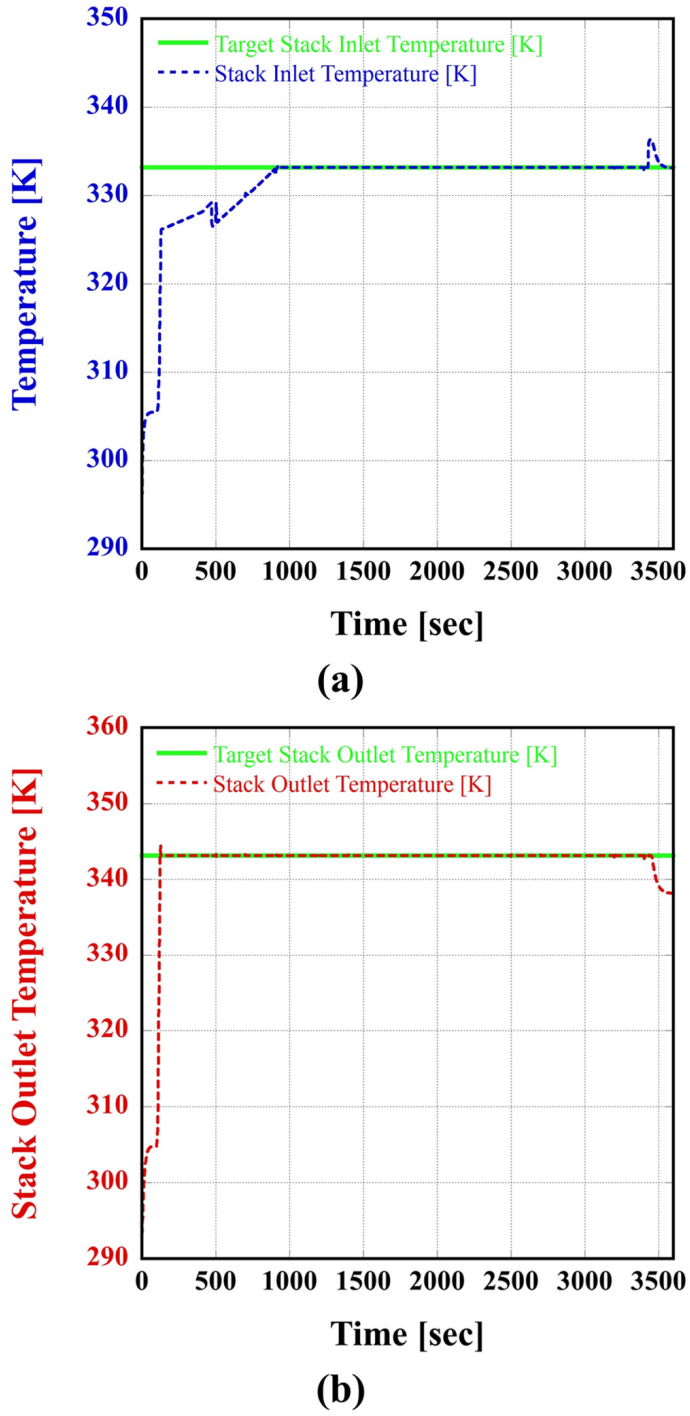

Figure 11. Temperature response results: (**a**) stack inlet temperature; (**b**) stack outlet temperature.

The heat generated from the fuel cell stack is cooled by the control of the distribution valve for the thermal management system and the metal hydride tank. As a result, the required heat release of the thermal management system decreases because of the heat

absorption process of the metal hydride tank, which is confirmed in Figure 12. After the first 100 s of the simulation, as the hydrogen fuel cell hybrid UAM system is flown, the load on the fuel cell system increases, and the required heat release increases accordingly. The thermal management system operates to control the temperature, but it can be confirmed that the hydrogen demand flow rate increases rapidly according to the load, as well as the heat required from the metal hydride tank. However, in the section after 900 s, it can be confirmed that the required heat decreases because of the increase in hydrogen generated from the metal hydride tank, as well as that the heat release occurs because of the operation of the thermal management system for temperature control. In addition, it can be confirmed that the heat release from the metal hydride tank reaches approximately 60% of the total heat release due to the rapid increase in the required hydrogen flow rate at the beginning of the simulation, as well as that it decreases to approximately 30% of the total heat release as the required heat from the metal hydride tank decreases thereafter. As a result, it can be confirmed that, on average, 43% of the waste heat is recovered through the tank as the hydrogen-fuel-cell–battery hybrid UAM system using hydrogen metal hydride is flown.

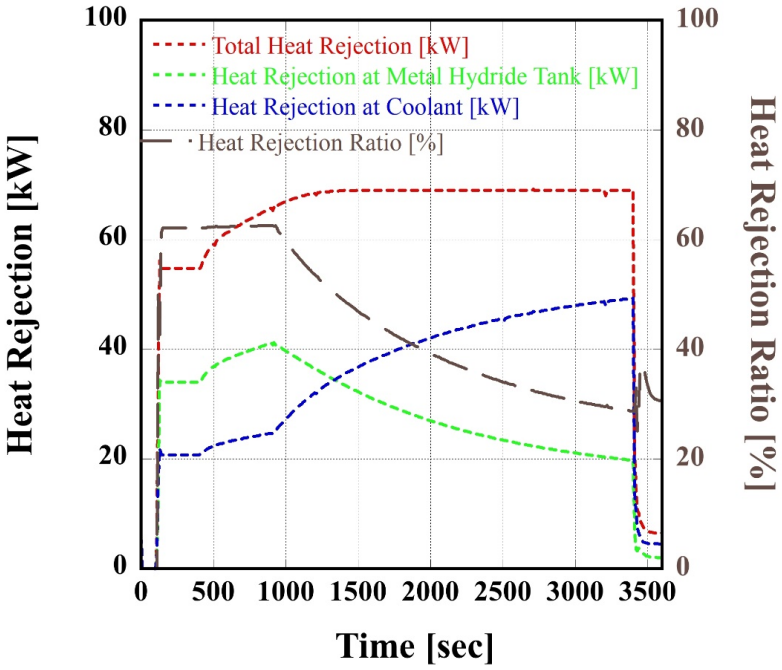

Figure 12. Comparison of the heat rejection at the metal hydride tank and coolant.

4. Conclusions

In this study, a model of a hydrogen fuel cell hybrid UAM system using a metal hydride tank was developed. The absorption reaction of the metal hydride tank using the waste heat generated from the stack was controlled through state machine control, and the power management system for the hybrid system was applied to the fuzzy logic control. The main results of this study are summarized as follows:

1. A hydrogen fuel cell hybrid UAM system was developed using a 138 kW FC gen-HPS-based fuel cell system from Ballard and a 60 kW battery;
2. A metal hydride tank system for the hydrogen supply was mathematically developed based on thermodynamic and energy conservation equations and applied to a hydrogen fuel cell system;
3. The absorption of heat for the desorption process of the metal hydride was applied through the waste heat generated from the fuel cell stack, and this was configured to be controlled by applying state machine control to the distribution valve;

4. A flight simulation was applied based on the Korean Urban Air Mobility (K-UAM) operation concept for the hydrogen fuel cell hybrid UAM system, and a power management system based on fuzzy logic control was developed and applied for efficient power distribution of the battery and hydrogen fuel cell system;
5. The load power was distributed by the fuzzy logic control-based power management system according to the flight scenario, and it was confirmed that 43% of the waste heat generated from the fuel cell stack was recovered through hydrogen metal cargo and hydrogen was desorbed.

Author Contributions: Model design: S.Y.; Methodology: S.Y.; Writing—original draft: S.Y.I. and J.H.; Supervision: S.Y.I. and J.H. All authors have read and agreed to the published version of the manuscript.

Funding: This work was supported by the research fund of Chungnam National University.

Data Availability Statement: Data are contained within the article.

Acknowledgments: This research was supported by "Regional Innovation Strategy (RIS)" through the National Research Foundation of Korea(NRF) funded by the Ministry of Education(MOE) (2021RIS-004). and This work was supported by the research fund of Chungnam National University.

Conflicts of Interest: The authors declare no conflict of interest.

Nomenclature

A	Active area [cm^2]
B	Viscous friction coefficient [N·m·s/rad]
E	Open-circuit voltage [V]
F	Faraday's constant [C/mol]
F	Force [N]
ΔG	Gibbs free energy change [J/mol]
Δh	Enthalpy [J/mol]
i	Current [A]
j	Current density [A/cm^2]
J	Moment of inertia [$kg \cdot m^2$]
Kt	Torque constant [Nm/A]
m	Mass [kg]
m	Mole flow rate [mol/s]
n	Number of electrons [-]
P	Pressure [bar]
p	Partial pressure [-]
R	Resistance [Ω]
R	Universal gas constant [J/K·mol]
stoi	Stoichiometric ratio [-]
T	Temperature [K]
V	Voltage [V]
v	Velocity [m/s]

Subscripts and superscripts

act	Activation
BT	Battery
conc	Concentration
conv	Converter
ohm	ohmic

Greek

α	Activity [-]
ρ	Density [kg/m^3]

References

1. Pukhova, A.; Llorca, C.; Moreno, A.; Staves, C.; Zhang, Q.; Moeckel, R. Flying taxis revived: Can Urban air mobility reduce road congestion? *J. Urban Mobil.* **2021**, *1*, 100002. [CrossRef]
2. Straubinger, A.; Rothfeld, R.; Shamiyeh, M.; Büchter, K.D.; Kaiser, J.; Plötner, K.O. An overview of current research and developments in urban air mobility–Setting the scene for UAM introduction. *J. Air Transp. Manag.* **2020**, *87*, 101852. [CrossRef]
3. Cohen, A.P.; Shaheen, S.A.; Farrar, E.M. Urban air mobility: History, ecosystem, market potential, and challenges. *IEEE Trans. Intell. Transp. Syst.* **2021**, *22*, 6074–6087. [CrossRef]
4. Melo, S.P.; Toghyani, S.; Cerdas, F.; Liu, X.; Gao, X.; Lindner, L.; Barke, A.; Thies, C.; Spengler, T.S.; Herrmann, C. Model-based assessment of the environmental impacts of fuel cell systems designed for eVTOLs. *Int. J. Hydrogen Energy* **2023**, *48*, 3171–3187. [CrossRef]
5. Kadyk, T.; Schenkendorf, R.; Hawner, S.; Yildiz, B.; Römer, U. Design of fuel cell systems for aviation: Representative mission profiles and sensitivity analyses. *Front. Energy Res.* **2019**, *7*, 440189. [CrossRef]
6. Ahmed, S.S.; Hulme, K.F.; Fountas, G.; Eker, U.; Benedyk, I.V.; Still, S.E.; Anastasopoulos, P.C. The flying car—Challenges and strategies toward future adoption. *Front. Built Environ.* **2020**, *6*, 106. [CrossRef]
7. Ma, S.; Lin, M.; Lin, T.E.; Lan, T.; Liao, X.; Maréchal, F.; Yang, Y.; Dong, C.; Wang, L. Fuel cell-battery hybrid systems for mobility and off-grid applications: A review. *Renew. Sustain. Energy Rev.* **2021**, *135*, 110119. [CrossRef]
8. Wang, F.C.; Gao, C.Y.; Li, S.C. Impacts of power management on a PEMFC electric vehicle. *Int. J. Hydrogen Energy* **2014**, *39*, 17336–17346. [CrossRef]
9. Curtin, D.E.; Lousenberg, R.D.; Henry, T.J.; Tangeman, P.C.; Tisack, M.E. Advanced materials for improved PEMFC performance and life. *J. Power Sources* **2004**, *131*, 41–48. [CrossRef]
10. Wang, F.C.; Peng, C.H. The development of an exchangeable PEMFC power module for electric vehicles. *Int. J. Hydrogen Energy* **2014**, *39*, 3855–3867. [CrossRef]
11. Li, X.; Ye, T.; Meng, X.; He, D.; Li, L.; Song, K.; Jiang, J.; Sun, C. Advances in the Application of Sulfonated Poly (Ether Ether Ketone) (SPEEK) and Its Organic Composite Membranes for Proton Exchange Membrane Fuel Cells (PEMFCs). *Polymers* **2024**, *16*, 2840. [CrossRef] [PubMed]
12. Tiwari, S.; Pekris, M.J.; Doherty, J.J. A review of liquid hydrogen aircraft and propulsion technologies. *Int. J. Hydrogen Energy* **2024**, *57*, 1174–1196. [CrossRef]
13. Jung, W.; Choi, M.; Jeong, J.; Lee, J.; Chang, D. Design and analysis of liquid hydrogen-fueled hybrid ship propulsion system with dynamic simulation. *Int. J. Hydrogen Energy* **2024**, *50*, 951–967. [CrossRef]
14. Smith, J.R.; Mastorakos, E. An energy systems model of large commercial liquid hydrogen aircraft in a low-carbon future. *Int. J. Hydrogen Energy* **2024**, *52*, 633–654. [CrossRef]
15. Lototskyy, M.V.; Tolj, I.; Pickering, L.; Sita, C.; Barbir, F.; Yartys, V. The use of metal hydrides in fuel cell applications. *Prog. Nat. Sci. Mater. Int.* **2017**, *27*, 3–20. [CrossRef]
16. Chabane, D.; Ibrahim, M.; Harel, F.; Djerdir, A.; Candusso, D.; Elkedim, O. Energy management of a thermally coupled fuel cell system and metal hydride tank. *Int. J. Hydrogen Energy* **2019**, *44*, 27553–27563. [CrossRef]
17. Rizzi, P.; Pinatel, E.; Luetto, C.; Florian, P.; Graizzaro, A.; Gagliano, S.; Baricco, M. Integration of a PEM fuel cell with a metal hydride tank for stationary applications. *J. Alloys Compd.* **2015**, *645*, S338–S342. [CrossRef]
18. Ahluwalia, R.K.; Peng, J.K.; Wang, X.; Papadias, D.; Kopasz, J. Performance and cost of fuel cells for urban air mobility. *Int. J. Hydrogen Energy* **2021**, *46*, 36917–36929. [CrossRef]
19. Kim, J.; Kwon, D.; Jeong, S. Conceptual design of hybrid electric vertical take-off and landing (eVTOL) aircraft with a liquid hydrogen fuel tank. *Prog. Supercond. Cryog. PSAC* **2022**, *24*, 27–38.
20. An, J.H.; Kwon, D.Y.; Jeon, K.S.; Tyan, M.; Lee, J.W. Advanced sizing methodology for a multi-mode EVTOL UAV powered by a hydrogen fuel cell and battery. *Aerospace* **2022**, *9*, 71. [CrossRef]
21. Santos, D.F.; Ferreira, R.B.; Falcão, D.S.; Pinto, A.M.F.R. Evaluation of a fuel cell system designed for unmanned aerial vehicles. *Energy* **2022**, *253*, 124099. [CrossRef]
22. Boukoberine, M.N.; Zhou, Z.; Benbouzid, M. A critical review on unmanned aerial vehicles power supply and energy management: Solutions, strategies, and prospects. *Appl. Energy* **2019**, *255*, 113823. [CrossRef]
23. Fakhreddine, O.; Gharbia, Y.; Derakhshandeh, J.F.; Amer, A.M. Challenges and solutions of hydrogen fuel cells in transportation systems: A review and prospects. *World Electr. Veh. J.* **2023**, *14*, 156. [CrossRef]
24. Kim, S.; Choi, Y.; Chang, D. Techno–economic analysis of fuel cell powered urban air mobility system. *Int. J. Hydrogen Energy* **2024**, *50*, 988–1004. [CrossRef]

25. Mazzeo, F.; Di Ilio, G. Fuel cell hybrid electric propulsion system for a lightweight helicopter: Design and performance analysis in urban air mobility scenario. *Int. J. Hydrogen Energy* **2024**, *50*, 891–907. [CrossRef]
26. Jia, C.; Zhou, J.; He, H.; Li, J.; Wei, Z.; Li, K.; Shi, M. A novel energy management strategy for hybrid electric bus with fuel cell health and battery thermal-and health-constrained awareness. *Energy* **2023**, *271*, 127105. [CrossRef]
27. Zheng, C.H.; Xu, G.Q.; Park, Y.I.; Lim, W.S.; Cha, S.W. Prolonging fuel cell stack lifetime based on Pontryagin's Minimum Principle in fuel cell hybrid vehicles and its economic influence evaluation. *J. Power Sources* **2014**, *248*, 533–544. [CrossRef]
28. Pereira, D.F.; da Costa Lopes, F.; Watanabe, E.H. Nonlinear model predictive control for the energy management of fuel cell hybrid electric vehicles in real time. *IEEE Trans. Ind. Electron.* **2020**, *68*, 3213–3223. [CrossRef]
29. Zhou, Y.; Ravey, A.; Péra, M.C. Real-time cost-minimization power-allocating strategy via model predictive control for fuel cell hybrid electric vehicles. *Energy Convers. Manag.* **2021**, *229*, 113721. [CrossRef]
30. He, H.; Jia, C.; Li, J. A new cost-minimizing power-allocating strategy for the hybrid electric bus with fuel cell/battery health-aware control. *Int. J. Hydrogen Energy* **2022**, *47*, 22147–22164. [CrossRef]
31. Chang, Z.; Fan, Y.; Jiang, W.; Zhang, J.; Zhang, J. Simulation Research on Thermal Management of Hydrogen Fuel Cell for UAV. In Proceedings of the International Conference on 6GN for Future Wireless Networks, Shanghai, China, 7–8 October 2023; Springer Nature: Cham, Switzerland, 2023; pp. 390–408.
32. He, Q.; Shen, J.; Dong, Z.; Liu, C.; Guo, X.; Zhao, X. Online Systemic Energy Management Strategy of Fuel Cell System with Efficiency Enhancement. *IEEE Trans. Transp. Electrif.* **2024**. [CrossRef]
33. Anselma, P.G.; Luciani, S.; Tonoli, A. Dynamic Programming for Thermal Management of Automotive Fuel Cell Systems: Investigating Hydrogen Saving Potential. *IEEE Access* **2023**, *11*, 48080–48098. [CrossRef]
34. Li, J.; Wu, T.; Cheng, C.; Li, J.; Zhou, K. A review of the research progress and application of key components in the hydrogen fuel cell system. *Processes* **2024**, *12*, 249. [CrossRef]
35. Darkrim, F.L.; Malbrunot, P.; Tartaglia, G.P. Review of hydrogen storage by adsorption in carbon nanotubes. *Int. J. Hydrogen Energy* **2002**, *27*, 193–202. [CrossRef]
36. Sakintuna, B.; Lamari-Darkrim, F.; Hirscher, M. Metal hydride materials for solid hydrogen storage: A review. *Int. J. Hydrogen Energy* **2007**, *32*, 1121–1140. [CrossRef]
37. Satheesh, A.; Muthukumar, P. Performance investigation of double-stage metal hydride based heat pump. *Appl. Therm. Eng.* **2010**, *30*, 2698–2707. [CrossRef]
38. Park, J.G.; Jang, K.J.; Lee, P.S.; Lee, J.Y. The operating characteristics of the compressor-driven metal hydride heat pump system. *Int. J. Hydrogen Energy* **2001**, *26*, 701–706. [CrossRef]
39. Kim, G.J.; Kim, G.Y.; Chae, J.U. A numerical study on a prediction of performance of the metal hydride thermal conversion system through the propagation phenomena of superadiabatic thermal waves. *Trans. Korean Soc. Mech. Eng. B* **2001**, *25*, 572–582.
40. Kikkinides, E.S.; Georgiadis, M.C.; Stubos, A.K. Dynamic modelling and optimization of hydrogen storage in metal hydride beds. *Energy* **2006**, *31*, 2428–2446. [CrossRef]
41. Massaro, M.C.; Biga, R.; Kolisnichenko, A.; Marocco, P.; Monteverde, A.H.A.; Santarelli, M. Potential and technical challenges of on-board hydrogen storage technologies coupled with fuel cell systems for aircraft electrification. *J. Power Sources* **2023**, *555*, 232397. [CrossRef]
42. Cho, J.H.; Yu, S.S.; Kim, M.Y.; Kang, S.G.; Lee, Y.D.; Ahn, K.Y.; Ji, H.J. Dynamic modeling and simulation of hydrogen supply capacity from a metal hydride tank. *Int. J. Hydrogen Energy* **2013**, *38*, 8813–8828. [CrossRef]
43. Available online: https://www.ballard.com/fcgen/ (accessed on 20 November 2024).
44. Hagag, N.; Jäger, F. Evaluation of the Technical Value of Powertrain Systems to Enable Safe Performance-based Flight Guidance for Urban Air Mobility. In Proceedings of the 2023 IEEE/AIAA 42nd Digital Avionics Systems Conference (DASC), Barcelona, Spain, 1–5 October 2023; IEEE: New York, NY, USA, 2023; pp. 1–11.
45. Garcia, P.; Fernandez, L.M.; Garcia, C.A.; Jurado, F. Fuel cell-battery hybrid system for transport applications. In Proceedings of the 2009 International Conference on Electrical Machines and Systems, Tokyo, Japan, 15–18 November 2009; IEEE: New York, NY, USA; pp. 1–5.
46. Chan, C.C. The state of the art of electric, hybrid, and fuel cell vehicles. *Proc. IEEE* **2007**, *95*, 704–718. [CrossRef]
47. Hyun, D.I.; Hong, S.M.; Han, J.Y. Model Development for Analysis of the System Dynamic Characteristics for Fuel Cell-Battery based Unmanned Aerial Vehicles. *J. Hydrog. New Energy* **2023**, *34*, 490–496. [CrossRef]
48. Wang, Y.; Sun, Z.; Chen, Z. Energy management strategy for battery/supercapacitor/fuel cell hybrid source vehicles based on finite state machine. *Appl. Energy* **2019**, *254*, 113707. [CrossRef]
49. Xu, L.; Ouyang, M.; Li, J.; Yang, F.; Lu, L.; Hua, J. Application of Pontryagin's Minimal Principle to the energy management strategy of plugin fuel cell electric vehicles. *Int. J. Hydrogen Energy* **2013**, *38*, 10104–10115. [CrossRef]

50. K_UAM Operation Concept. Available online: https://www.molit.go.kr/USR/NEWS/m_71/dtl.jsp?id=95086041 (accessed on 20 November 2024).
51. Corcau, J.I.; Dinca, L.; Cican, G.; Ionescu, A.; Negru, M.; Bogateanu, R.; Cucu, A.A. Studies Concerning Electrical Repowering of a Training Airplane Using Hydrogen Fuel Cells. *Aerospace* **2024**, *11*, 218. [CrossRef]